JPE 17-5-4

https://doi.org/10.6113/JPE.2017.17.5.1160
ISSN(Print): 1598-2092 / ISSN(Online): 2093-4718

Research on a Multi-level Space Vector Modulation Strategy in Non-orthogonal Three-dimensional Coordinate Systems

Chuan-Jin Zhang†, Rui-Peng Wei*, Yi Tang*, and Ke Wang*

†,*School of Electrical and Power Engineering, China University of Mining and Technology, Xuzhou, China

Abstract

A novel space vector modulation strategy in the non-orthogonal three-dimensional coordinate system for multi-level three-phase four-wire inverters is proposed in this paper. This new non-orthogonal three-dimensional space vector modulation converts original trigonometric functions in the orthogonal three-dimensional space coordinate into simple algebraic operations, which greatly reduces the algorithm complexity of three-dimensional space vector modulation and preserves the independent control of the zero-sequence component. Experimental results have verified the correctness and effectiveness of the proposed three-dimensional space vector modulation in the new non-orthogonal three-dimensional coordinate system.

Key words: Multi-level, Non-orthogonal three-dimensional coordinate system, Three-dimensional space vector modulation

I. INTRODUCTION

In recent years, three-phase four-wire inverters have been widely used in active power filters (APFs) [1]-[8], uninterruptible power supplies (UPSs)[9], renewable energy power generation [10], [11] and power conversion devices in three-phase four-wire power supply systems due to their ability to produce zero-sequence voltage. Three-phase four-wire inverters mainly include two topologies [2]: three-leg inverters and four-leg inverters, which are shown in Fig. 1(a) and (b), respectively. The three-leg inverters directly connect the neutral-point (NP) of dc-link capacitors and the neutral point of the power system to construct a fourth wire. Thus, they are also referred as three-leg center-split capacitor (TLSC) inverters [1]. Four-leg converters have a better zero-sequence compensation effect than three-leg converters. However, their main circuit needs more switch devices, which greatly increases the cost [12]. In this paper, the study object is a three-level TLSC inverter as shown in Fig.1(a).

The pulse width modulation (PWM) strategy is a key technology in the control of multi-level three-phase four-wire inverters. Various PWM strategies for multilevel inverters have been studied and a lot of results have published such as carrier-based modulation (CBM) [13]-[15], space vector modulation (SVM) [16]-[18] and a number of PWMs with specific functions [19]-[22]. However, these traditional PWM strategies are all realized on the two-dimensional (2D) plane. With these strategies, it is difficult to output and control the zero-sequence component of reference voltage. Therefore, the study of the PWM strategies for three-phase four-wire inverters mostly focuses on the three-dimensional (3D) modulation algorithm [1]-[11], [23]-[31]. The three-leg center-split capacitor topology was first presented in [23], and a 3D hysteresis modulation was proposed for pulse control. The 3D hysteresis modulation is simple and easy to implement. However, its switching frequency is not fixed. In order to overcome the drawback of 3D hysteresis modulation, a fixed switching frequency 3D hysteresis, which was realized by the real-time changing of the hysteresis width with a look-up table, was proposed in [24]. However, the design of the look-up table is quite complex. A carrier-based PWM technique extending the offset voltage concepts to the three-phase four-wire converter is equivalent to the symmetrically aligned three-dimensional space vector modulation (3D-SVM) [25]. However, the appropriate offset voltage injection requires complex calculations and is only

Manuscript received Oct. 5, 2016; accepted May 9, 2017
Recommended for publication by Associate Editor Sangshin Kwak.
†Corresponding Author: chuanjin2359@163.com
Tel: +86-13913451470, China University of Mining and Technology
*School of Electrical and Power Engineering, China University of Mining and Technology, China

suitable for four-leg converters. Compared with other modulation strategies for three-phase three-wire inverters, the 3D-SVM strategy is a high-quality PWM control method that offers many advantages such as a low output distortion, high bus voltage utilization and digital implementation simplicity. Therefore, a three-dimensional space vector modulation (3D-SVM) suitable for three-phase four-wire converters has been extensively studied. Two types of 3D-SVM based on the α-β-γ and a-b-c coordinate systems have been developed. The first 3D-SVM, based on the α-β-γ coordinate system, was proposed for two-level three-leg center-split capacitor inverters [1]. Then based on the 3D-SVM proposed in [1], a symmetrical components control method was added to improve the control effect under unbalanced conditions [26], [27]. The authors of [28] expanded the α-β-γ 3D-SVM to three-level TLSC inverters, and offered a simple control method for the NP potential balance. The algorithm complexity of the α-β-γ 3D-SVM for TLSC inverters increases dramatically with an increase in the number of levels. Many studies have been dedicated to simplifying the three-level 3D-SVM based on the α-β-γ coordinate system to a two-level 3D-SVM [2], [3], [5]. This approach plays a certain role in reducing algorithm complexity. However, it still has many limitations when applied to multi-level converters. To solve these problems, some scholars have established a three-phase orthogonal a-b-c 3D coordinate system, and done research on 3D-SVM for multi-level three-phase four-wire inverters in this coordinate system [5], [6], [29]-[31]. The 3D-SVM based on the a-b-c coordinate system does not require multiplication or trigonometric operations when calculating the duration of vectors. Therefore, it is simple and easy to expand to higher-order topologies when compared with the α-β-γ 3D-SVM. However, the a-b-c 3D-SVM does not separate the symmetrical and asymmetrical components very well. Moreover, the NP potential control is relatively complicated in this 3D-SVM. The authors of [7], [32], [33] analyzed the duty cycle of 3D space vectors and proposed a 3D direct pulse width modulation (3D-DPWM) strategy that is similar to the 3D-SVM strategy based on the a-b-c coordinate system. Besides, a simple NP potential control method has been added to the 3D-DPWM. Recently a hybrid 2D and 3D SVM strategy that is suitable for both balanced and unbalanced conditions was presented in [11]. Further analysis of the mathematical description and the inverter output voltage distortion of the hybrid SVM have been conducted in [34]. However, the modulation section of the hybrid SVM is still performed in the α-β-γ coordinate system. Thus, the contradiction between the calculation complexity and the control flexibility zero-sequence voltage is still unresolved.

A novel 3D-SVM strategy which is suitable for multi-level TLSC inverters is proposed in this paper. Based on comparing and analysing two traditional coordinate systems (α-β-γ and a-b-c), a novel non-orthogonal three-dimensional coordinate system (K-L-0) integrating the advantages of both of the classical coordinate systems is introduced in this paper. The novel non-orthogonal 3D-SVM is established in the K-L-0 coordinate system. In additional, in terms of the inherent neutral-point (NP) voltage unbalance of the multi-level TLSC inverter, a simple NP voltage control strategy is replenished in the non-orthogonal 3D-SVM. Finally, experiments are conducted on the three-level TLSC inverter and the correctness and feasibility of the proposed new 3D modulation strategy have been verified.

II. Non-Orthogonal Three-Dimensional Coordinate System

A. Novel Coordinate System

In order to improve the research of the 3D-SVM for three-phase four-wire multi-level inverters, a reasonable three-dimensional coordinate system should be established first. In previous studies the most commonly used three-dimensional coordinate systems can be divided into two types: α-β-γ and a-b-c coordinate systems.

Coordinate transformations from the ABC to α-β-γ coordinate systems well separate the symmetrical components (positive-sequence and negative-sequence components) and asymmetrical component (zero-sequence component) of any space voltage vector. Therefore, space vectors in the α-β-γ coordinate system have definitude physical meanings and the zero-sequence component of these vectors can be directly represented by the γ-axis coordinate. This will allow the α-β-γ 3D-SVM to have greater flexibility in terms of NP voltage balance and zero-sequence voltage output. However, the 3D modulation algorithm implemented in this coordinate is very complex and requires lots of trigonometric functions and coordinate translation operations, which greatly increases the system consumption and cost. In addition, this 3D modulation algorithm is difficult to expand to multi-level inverter applications.

Going from the ABC to the a-b-c 3D coordinate system does not need any coordinate transformation, because the a-b-c 3D coordinate system is just a spatial expression of the ABC three-phase voltage. The symmetric and asymmetric components of the space vectors in the a-b-c coordinate system are not separated and cannot be directly represented by coordinates of three-axes. This means that there is still coupling between the three coordinate variables of the space vector in the a-b-c 3D coordinate system. The 3D-SVM based on the a-b-c coordinate system does not require complex trigonometric functions or coordinate transformation when selecting combined vectors as well as calculating the dwell time of the selected vectors. Thus, it overcomes the shortcomings of the large computation of the α-β-γ 3D-SVM. Besides, the 3D-SVM based on the a-b-c coordinate system is

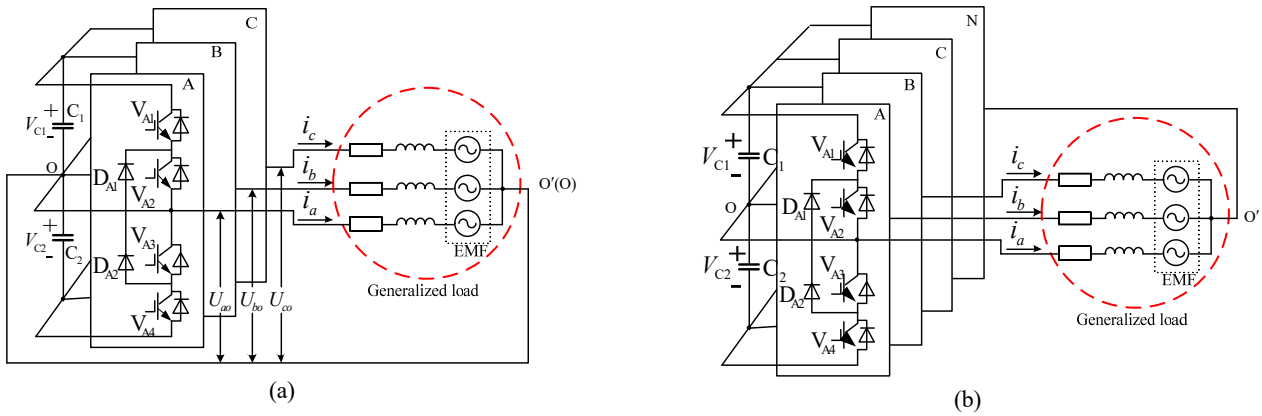

Fig. 1. Circuits of three-level three-phase four-wire inverters: (a) three-leg center-split capacitor; (b) four-leg center-split capacitor.

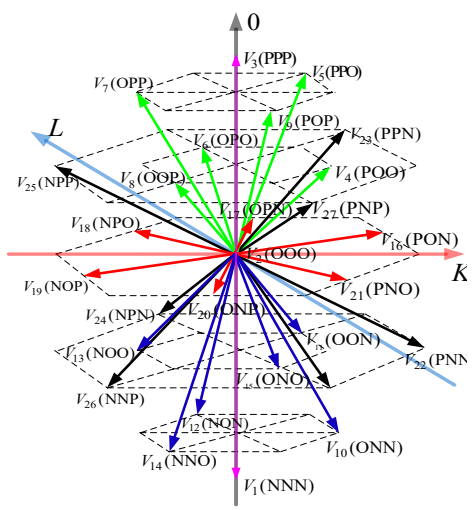

(a) K-L-0 coordinate system.

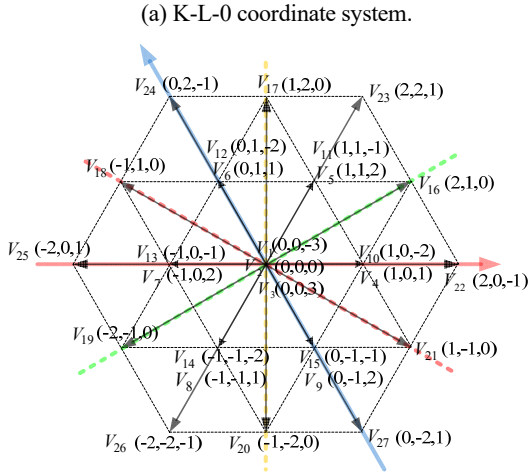

(b) K-L plane.

Fig. 2. Distribution of basic space vectors in the K-L-0 coordinate system and projections on the K-L plane.

easy to expand to circuit topologies with more levels. However, the coupling relations among the three axes coordinates make the control of the zero-sequence voltage output and the NP voltage balance relatively complex.

Although there is a great difference between the two three-dimensional coordinate systems, both of them have orthogonal characteristics. In order to integrate the advantages of the two traditional coordinate systems, a novel non-orthogonal three-dimensional coordinate system (K-L-0) is introduced in this paper. In this system, the K-L axis locates on the α-β plane, and the K-axis coincides with the α-axis, the L-axis leads the β-axis π/6, and the 0-axis coincides with the γ-axis. The transformation coefficient matrix from the ABC three-phase to the K-L-0 non-orthogonal three-dimensional coordinate system is presented in equation (1). Here, all of the coordinate transformations are used in the proportional transformation for description convenience.

$$\begin{bmatrix} U_K \\ U_L \\ U_0 \end{bmatrix} = \begin{bmatrix} 1 & 0 & -1 \\ 0 & 1 & -1 \\ 1 & 1 & 1 \end{bmatrix} \begin{bmatrix} U_a \\ U_b \\ U_c \end{bmatrix} \tag{1}$$

Three-level three-leg center-split capacitor inverters have 27 different switching combinations, which correspond to 27 different space vectors in the 3D coordinate system. The distribution of all of the space vectors in the K-L-0 coordinate system and the projections of these vectors on the K-L plane are shown in Fig. 2.

Assume that the voltage of dc-linked capacitors are same and equal to half of the voltage on the DC bus ($1/2u_{dc}$). Then use $1/2u_{dc}$ to get the p.u. values of the terminal voltage u_{xo}(x=a,b,c) shown in Fig. 2(a). It can be concluded that: U_{xo} =1, when the switching state of the X-phase (X=A, B, C) is "P"; u_{xo}=0, when the switching state of the X-phase is "O"; and u_{xo}=-1, when the switching state of the bridge arm X-phase is "N". The corresponding K-L-0 coordinates of the 27 fundamental voltage space vectors are marked in the K-L plane as shown in Fig. 2(b). For calculation convenience, proportional transformation is used in this article so that the coordinate units for each of the axis in Fig. 2 are not perfectly equivalent, where the units of the K and L axes are $1/3u_{dc}$, and the unit of the 0 axis is $1/6u_{dc}$.

B. Equivalent Analysis of Different Coordinate Systems

From Fig. 2, the distribution of the 27 basic space vectors in the K-L-0 coordinate system are entirely consistent with those of the α-β-γ coordinate system, and all of these vectors

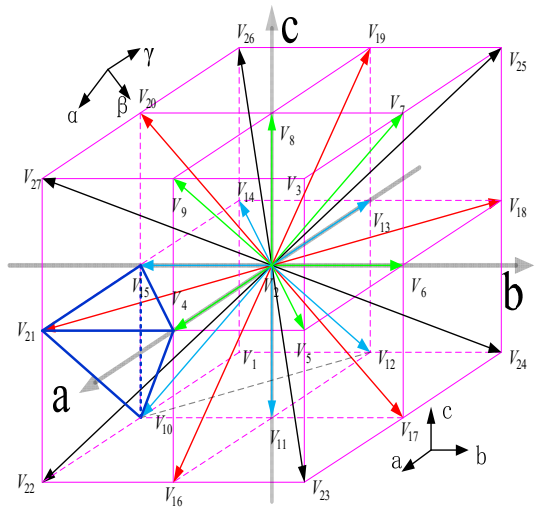

(a) a-b-c.

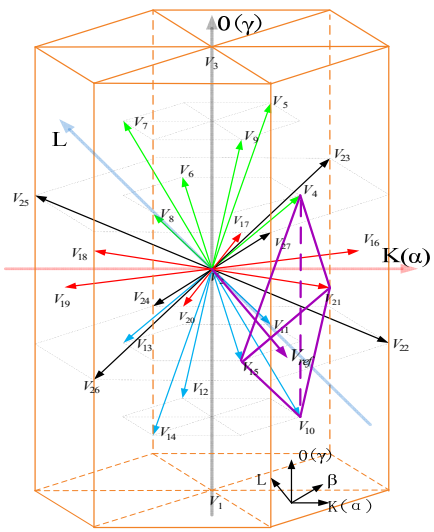

(b) K-L-0 (α-β-γ).

Fig. 3. Distribution of basic space vectors in different coordinate systems.

sequentially distribute in a regular hexagonal prism [3], [8], [25]. While in the a-b-c 3D coordinate system, the corresponding basic space vectors are located in eight cubes whose directions are opposite [27], [28]. The distribution and mutual correspondence relationship of all 27 space vectors in the α-β-γ, K-L-0 and a-b-c coordinate systems are shown in Fig. 3.

Any form of coordinate transformation is an affine transformation which can be achieved by compounding five basic sub transformations, such as: Translation, Scale, Flip, Rotation and Shear. The affine transformation preserves collinearity, flatness, parallelism, and ratios of distances. Therefore, a straight line (or plane) is transformed into another straight line (or plane). If a point divides a line in a given ratio, the transformed point divides the transformed line in the same ratio [9]. The coordinate transformation from the a-b-c to the K-L-0 non-orthogonal coordinate system shown in equation (1) can be further decomposed into equation (2).

Where, $T_{\alpha\beta\gamma}$ is the coefficient matrix of the Clark transformation, and T_1 is the coefficient matrix of the transformation from the α-β-γ to the K-L-0 coordinate systems. Obviously T_1 is a full rank matrix. Therefore, there must be only one $[U_K, U_L, U_0]^T$ in the K-L-0 coordinate system corresponding to the arbitrary vector $[U_\alpha, U_\beta, U_\gamma]^T$ in the α-β-γ coordinate system. Beyond that, T_1 is also a combination of a scaling and a sheer transformation.

$$\begin{bmatrix} U_K \\ U_L \\ U_0 \end{bmatrix} = \begin{bmatrix} \frac{3}{2} & 0 & 0 \\ 0 & \sqrt{3} & 0 \\ 0 & 0 & 3 \end{bmatrix} \begin{bmatrix} 1 & \frac{1}{\sqrt{3}} & 0 \\ 0 & 1 & 0 \\ 0 & 0 & 1 \end{bmatrix} * \frac{2}{3} \begin{bmatrix} 1 & -\frac{1}{2} & -\frac{1}{2} \\ 0 & \frac{\sqrt{3}}{2} & -\frac{\sqrt{3}}{2} \\ \frac{1}{2} & \frac{1}{2} & \frac{1}{2} \end{bmatrix} \begin{bmatrix} U_a \\ U_b \\ U_c \end{bmatrix} = T_1 * T_{\alpha\beta\gamma} \begin{bmatrix} U_a \\ U_b \\ U_c \end{bmatrix} = T_1 \begin{bmatrix} U_\alpha \\ U_\beta \\ U_\gamma \end{bmatrix} \quad (2)$$

This means there are two steps from the α-β-γ to the K-L-0 coordinate system, and the two steps are as follows:

1) Sheer the β-axis to the K-axis.

2) Scale the object obtained in step 1) along the three axes by $\frac{3}{2}$, $\sqrt{3}$ and 3, respectively.

Firstly, Clark transform matrix $T_{\alpha\beta\gamma}$ is a full rank matrix. Then it can be split into equation (3) in terms of sub transformations.

$$T_{\alpha\beta\gamma} = \frac{2}{3} \begin{bmatrix} 1 & -\frac{1}{2} & -\frac{1}{2} \\ 0 & \frac{\sqrt{3}}{2} & -\frac{\sqrt{3}}{2} \\ \frac{1}{2} & \frac{1}{2} & \frac{1}{2} \end{bmatrix} = \begin{bmatrix} 1 & 0 & 0 \\ 0 & \frac{\sqrt{2}}{2} & -\frac{\sqrt{2}}{2} \\ 0 & \frac{\sqrt{2}}{2} & \frac{\sqrt{2}}{2} \end{bmatrix} \begin{bmatrix} \frac{\sqrt{6}}{3} & 0 & -\frac{\sqrt{3}}{3} \\ 0 & 1 & 0 \\ \frac{\sqrt{3}}{3} & 0 & \frac{\sqrt{6}}{3} \end{bmatrix} \begin{bmatrix} \frac{\sqrt{6}}{3} & 0 & 0 \\ 0 & \frac{\sqrt{6}}{3} & 0 \\ 0 & 0 & \frac{\sqrt{3}}{3} \end{bmatrix} \quad (3)$$

$$= \begin{bmatrix} 1 & 0 & 0 \\ 0 & \cos\frac{\pi}{4} & -\sin\frac{\pi}{4} \\ 0 & \sin\frac{\pi}{4} & \cos\frac{\pi}{4} \end{bmatrix} * \begin{bmatrix} \cos 0.1959\pi & 0 & -\sin 0.1959\pi \\ 0 & 1 & 0 \\ \sin 0.1959\pi & 0 & \cos 0.1959\pi \end{bmatrix} * \begin{bmatrix} \frac{\sqrt{6}}{3} & 0 & 0 \\ 0 & \frac{\sqrt{6}}{3} & 0 \\ 0 & 0 & \frac{\sqrt{3}}{3} \end{bmatrix}$$

In equation (3), the affine transformation from the a-b-c coordinate system to the α-β-γ coordinate system consists of three steps[9]:

1) Rotate the a-b-c coordinate around the a-axis by π /4 radians in the counterclockwise direction.

2) Rotate the coordinate system obtained in step 1) around the b-axis by 0.1959π radians

3) Scale the object obtained in step 2) by $\sqrt{6}/3$ along the a and b-axes and by $\sqrt{3}/3$ along the c-axis. Then the α-β-γ coordinate system can be obtained.

The characteristic of the affine transformation ensures that the relative position and distance proportions for all of the vectors (including the basic and reference vectors) in the different coordinate systems are kept unchanged. Therefore, the 3D-SVM has an equivalent result in three different coordinate systems. For example, if the reference voltage space vector locates in the blue tetrahedron shown in Fig. 2(a), then after the coordinate transformation it locates in the

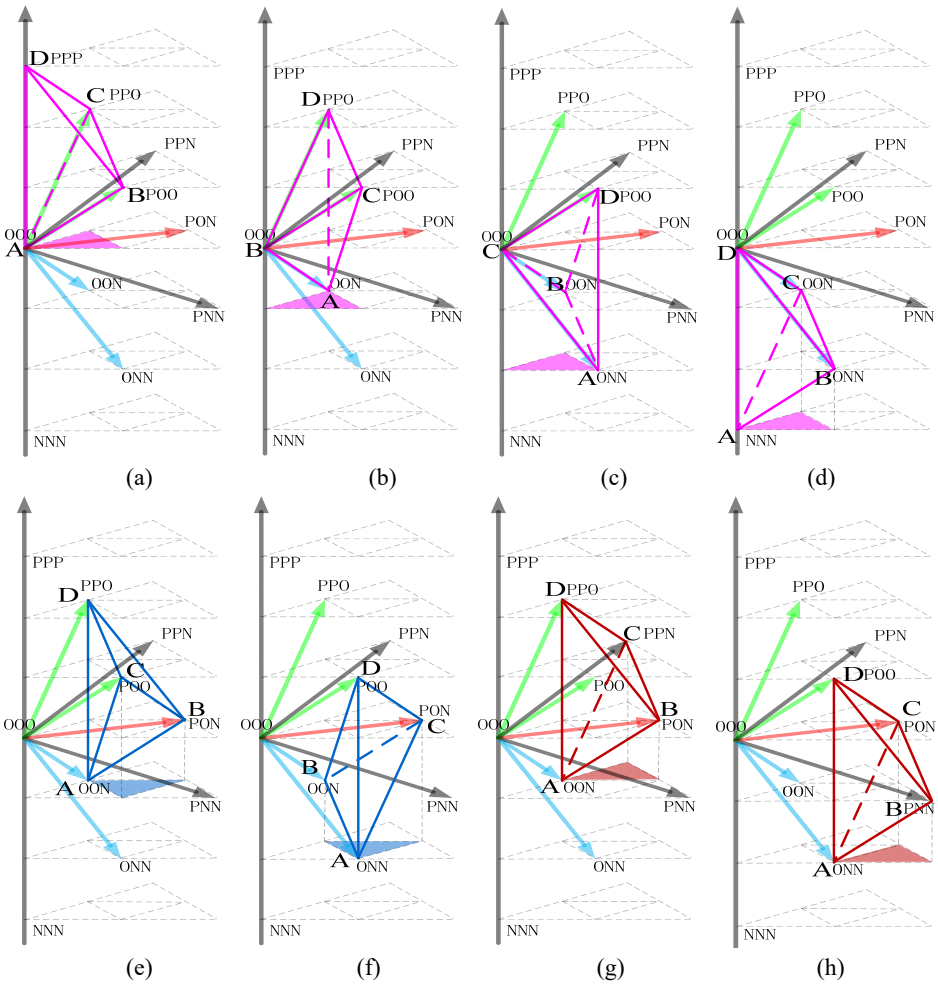

Fig. 4. Basic units within the first triangular prism.

blue tetrahedron presented in Fig. 2(b). Although the relative position of the tetrahedrons in the coordinate system has changed, the four basic space vectors which construct the tetrahedron remain unchanged and the distance proportions of the reference voltage and basic vectors are also kept constant. It can be concluded that the output of the reference voltage only depends on the switching state and duration time, regardless of the coordinate system.

III. NON-ORTHOGONAL THREE-DIMENSIONAL SVM

No matter which 3D coordinate system is used, the vertices of four adjacent basic space vectors can be connected to form a tetrahedron. For example, tetrahedrons composed of the vectors V_4(POO), V_{10}(ONN), V_{21}(PNO) and V_{15}(ONO) in different coordinate systems are presented in Fig.3. In classical 3D-SVMs, the four basic voltage vectors nearest tothe reference vector are commonly selected to compose the reference vector [2]-[6], [29]-[31]. The entire 3D space can be divided into 48 tetrahedrons according to the distribution of the 27 basic space vectors. According to solid geometry, the vertex of the reference vector just falls in the tetrahedron formed by the vertexes of four selected basic vectors. Therefore, finding the tetrahedron which contains the vertex of the reference vector will obtain the nearest four basic space vectors used to compose the reference vector. In this paper, each tetrahedron consist of the adjacent four basic space vectors is called a basic unit for synthesizing the reference vector.

It is necessary to further study these basic units in the K-L-0 coordinate system. Since all of the 27 space vectors distribute symmetrically in 3D space, it only needs to consider the basic units within the first triangular prism to cover all of the types. All of the basic units in the first triangular prism are illustrated in Fig. 4.

First, define a vertex with the smallest 0-axis coordinate in a basic unit as the datum point of this basic unit and the datum point is represented by a capital letter A, as shown in Fig. 4. Although the eight basic units within the first triangular prism are not completely consistent with each other, they have some similarities: (1) the four vertexes of each basic unit are located on a different 0-axis component plane; (2) the datum point and vertex with a maximum 0-axis

component have the same K and L axes coordinates. According to the projection of the eight basic units shown in Fig.4, the first large triangular prism can be divided into four small triangular prisms P_{I1}-P_{I4}, and the space expressions of P_{I1}-P_{I4} are shown as equation (4).

$$P_{I1}=\begin{cases}K<1\\L>0\\K>L\end{cases}\quad P_{I2}=\begin{cases}K>1\\L<1\\K-1<L\end{cases}\quad P_{I3}=\begin{cases}K<2\\L>1\\K>L\end{cases}\quad P_{I2}=\begin{cases}K<2\\L>0\\K-1>L\end{cases}\tag{4}$$

The eight basic units distributed in P_{I1}-P_{I4} can be divided into three categories based on their spatial vertical distance to the 0-axis. (1) The purple tetrahedron nearest the 0-axis, which is formed by a small vector and a zero vector, is called the center basic unit, and the ones located in P_{I1} are shown in Fig. 3(a)-(d). (2) The blue tetrahedron, which has a smaller spatial vertical distance to the 0-axis and is formed by a small vector and a middle vector, is called the middle basic unit, and the ones located in P_{I2} are illustrated in Fig. 4(e) and (f). (3) The red tetrahedron farthest away from the 0-axis, which is formed by a small vector, a middle vector and a large vector, is called the edge basic unit, and the ones located in P_{I3} and P_{I4} are shown in Fig. 4(g) and (h).

A. Determination of Basic Unit

It is not difficult to determine that to select the appropriate space vectors to construct the reference voltage vector, the specific basic unit wereh the reference voltage resides should be determined first. Select (*int* (U_K), *int* (U_L)) as the K and L axes coordinates of the datum point of the possible basic unit were the reference vector is located, where *int*(*) is an integral function which removes the fractional part of the input data. If (*int* (U_K), *int* (U_L))≠(0,0), the corresponding switch status [S_a, S_b, S_c] of the vectors [*int* (U_K), *int* (U_L), -2]^T and [*int* (U_K), *int* (U_L),-1]^T can be obtained by left multiplying the inverse matrix of equation (1). If $S_x\in\{-1, 0, 1\}$ (x=a, b, c) the vectors are selected as the datum point vector, and the vertex of this vector is regarded as a possible datum point.

Among the eight basic units within the first large triangular prism shown in Fig.4, the edge basic unit located in P_{I3} and P_{I4} has only one tetrahedron in the 0-axis direction, the middle basic units located in P_{I2} have two tetrahedrons in the 0-axis direction and they have the same projection on the KL-plane, while the center basic units located in P_{I1} have four such tetrahedrons in the 0-axis direction. This means the vertex of the reference voltage vector just locates in the edge basic unit, otherwise the datum point of the basic unit where the reference voltage vector locates in cannot be completely determined by only the K and L axis components of the reference voltages. Therefore, the datum point should be further corrected with the 0-axis component of the reference vector. Fig. 5 shows two reference voltage vectors V^1_{ref} =[U_{K1},U_{L1},U_{01}]^T and V^2_{ref}=[U_{K2},U_{L2},U_{02}]^T which are both located in P_{I2}, where U_{K1}=U_{K2}, U_{L1}=U_{L2} and U_{01}>U_{02}.

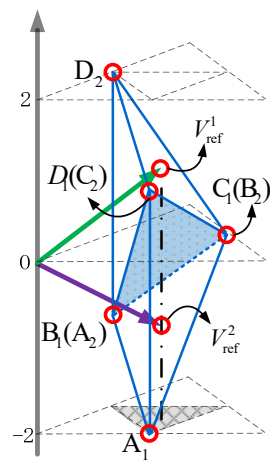

Fig. 5. Basic units within the first triangular prism.

TABLE I
RELATIONS BETWEEN THE BASIC UNIT VERTEXES

Conditions for component	Vector coordinates		
	V_B	V_C	V_D
K>0, L>0, K>L	V_A +[1,0,1]^T	V_B +[0,1,1]^T	
K>0,L>0, K<L	V_A +[0,1,1]^T	V_B +[1,0,1]^T	
K>0,L<0	V_A +[1,0,1]^T	V_B +[0,-1,1]^T	V_A +[0,0,3]^T
K<0,L<0, K<L	V_A +[-1,-1,1]^T	V_B +[-1,0,1]^T	
K<0,L<0, K>L	V_A +[-1,-1,1]^T	V_B +[0,-1,1]^T	
K<0,L>0	V_A +[0,1,1]^T	V_B +[-1,0,1]^T	

Although V^1_{ref} and V^2_{ref} have the same K and L axes components, the two reference vectors are located in different basic units of $A_2B_2C_2D_2$ =[(1,1,-1), (1,0,1), (2,1,0), (1,1,2)] and $A_1B_1C_1D_1$=[(1,0,-2), (1,1,-1), (1,0,1), (2,1,0)].

In Fig. 5 the two basic units $A_1B_1C_1D_1$ and $A_2B_2C_2D_2$ are located on two sides of the plane $B_1C_1D_1$=[(1,1,-1), (1,0,1), (2,1,0)]. Finally, the correct basic unit where the reference voltage vector locates in can be determined by judging the relative position between U_0 and the plane $B_1C_1D_1$. The equation of the $B_1C_1D_1$ plane can be expressed as S=2*|U_K-1|+|U_L-1|. If 2*|U_K-1|+|U_L-1|>U_0+1, then the reference vector coordinates are located within the tetrahedron $A_2B_2C_2D_2$; otherwise the reference vector coordinates are located within the tetrahedron $A_1B_1C_1D_1$ when 2*|U_K-1|+|U_L-1|<U_0+1 is satisfied.

When the datum point has completed the correction an offset vector [U_K-*int*(U_K), U_L-*int* (U_L), U_0-Y]^T can be obtained by subtracting the datum point vector from the reference voltage vector, where Y=-1 or -2. Then the reference voltage vector is shifted to a new space coordinate with the datum point as the coordinate origin. Moreover, according to the K

TABLE II
COMPONENTS OF THE MODIFIED BASIC VECTORS

Modified vectors	Position of the plane	K-axis component	L-axis component	**0**-axis component
V_{AB}	L=A(2)	1	0	1
	K=A(1)	0	1	1
	K=L	1	1	1
V_{AC}	L=A(2)	1	0	2
	K=A(1)	0	1	2
	K=L	1	1	2
V_{AD}	K=A(1)&L=A(2)	0	0	3

and L axes coordinates of the offset vector, the coordinates of the other three vertices of the basic unit with A=[*int* (U_K), *int* (U_L), Y]^T as the datum point can be obtained as shown in Table I. Once the basic unit containing the reference vector is determined, the four basic space vectors used to synthesize the reference voltage vector are selected.

B. Computation of the Vector Duration Time

According to the principle of the volt-second balance, there is a linear relationship between the reference voltage space vector and the selected basic voltage space vectors as shown in equation (5).

$$\begin{cases} V_{\text{ref}} T_S = V_A t_1 + V_B t_2 + V_C t_3 + V_D t_4 \\ t_i = d_i T_S, i = 1,2,3,4, \sum d_i = 1 \end{cases} \tag{5}$$

Where T_S is the switching period, t_1, t_2, t_3, t_4 represent the duration times of the space vectors V_A, V_B, V_C, V_D , and d_1, d_2, d_3, d_4 are the respective duty cycles. Here, V_A,V_B,V_C,V_D represent the four vertexes vectors of the basic unit where the reference vector is located. In order to facilitate the calculation, the reference vector is still translated into the coordinate system with the datum point as the coordinate origin. Then equation (5) can be rewritten as (6).

$$\begin{cases} V_{\text{ref}}^* = V_{AB} d_2 + V_{AC} d_3 + V_{AD} d_4 \\ d_1 = 1 - d_2 - d_3 - d_4 \end{cases} \tag{6}$$

Where V^*_{ref}=V_{ref}-V_A, V_{AB} =V_B-V_A, V_{AC} =V_C-V_A, V_{AD} =V_D-V_A. In the new coordinate system, the modified basic vector V_{AD} only contains the 0-axis component while V_{AB}, V_{AC} are more complex. The three axes components for all of the modified basic vectors are shown in Table II.

Where, A(x)(x=1, 2) are the K-axis and L-axis components of datum point A. Although the space position and geometry of the eight basic units in the first large triangular prism are not exactly the same, it is inevitable that the modified vectors V_{AB} and V_{AC} are in different space planes. From Table II, it can be found that at least one of V_{AB} and V_{AC} contains only the K-axis or L-axis component. However, the other one may contain both K-axis and L-axis components or only one component, depending on the plane where the modified space vector is located. Taking the basic unit in Fig.4 (f) as an example: V_{AB} only contains the L-axis component, V_{AC} contains both K-axis and L-axis components, and V_{AB}, V_{AC}, V_{AD} all contain the 0-axis component.

TABLE III
DUTY CYCLES OF THE BASIC VECTORS USED FOR CONSTITUTING THE REFERENCE VECTOR

Positional relationship	V_{AB} in L=A (2) plane	V_{AB} in K=A (1) plane	V_{AB} in K=L plane
V_{AC} in L=A (2) plane	Inactive state	$d_2 = V^*_{ref}(2)$ $d_3 = V^*_{ref}(1)$ $d_4 = V^*_{ref}(3) - 2d_2 - d_1$	$d_2 = V^*_{ref}(2)$ $d_3 = V^*_{ref}(1) - d_1$ $d_4 = V^*_{ref}(3) - 2d_2 - d_1$
V_{AC} in K=A(2) plane	$d_2 = V^*_{ref}(1)$ $d_3 = V^*_{ref}(2)$ $d_4 = V^*_{ref}(3) - 2d_2 - d_1$	Inactive state	$d_2 = V^*_{ref}(1)$ $d_3 = V^*_{ref}(2) - d_1$ $d_4 = V^*_{ref}(3) - 2d_2 - d_1$
V_{AC} in L=K plane	$d_2 = V^*_{ref}(1) - d_2$ $d_3 = V^*_{ref}(2)$ $d_4 = V^*_{ref}(3) - 2d_2 - d_1$	$d_2 = V^*_{ref}(2) - d_2$ $d_3 = V^*_{ref}(1)$ $d_4 = V^*_{ref}(3) - 2d_2 - d_1$	Inactive state

Therefore, the K-axis component of the reference vector V^*_{ref} (1) is uniquely represented by V_{AC}; the L-axis component V^*_{ref} (2) is represented by both V_{AB} and V_{AC}; and the 0-axis component V^*_{ref}(3) is represented by V_{AB}, V_{AC} and V_{AD} together.

$$\begin{cases} d_1 = 1 - d_2 - d_3 - d_4 \\ d_2 = V^*_{ref}(1) - V^*_{ref}(2) \\ d_3 = V^*_{ref}(2) \\ d_4 = V^*_{ref}(3) - V^*_{ref}(1) - V^*_{ref}(2) \end{cases} \tag{7}$$

As a result, based on the characteristics for each of the axis components contained by the modified basic vectors, the duration time of each basic vector is obtained by determination of the spatial position of the modified vector and simple algebraic operations as shown in Table III. For example, in Fig. 4(f) the duty cycles of V_A,V_B,V_C,V_D can be directly obtained as equation (7).

C. Determination of the Switching Sequence

After obtaining the duration time of the selected basic vectors, the final output switching states can be determined. However, different combinations of the switching sequence bring different results. The pros and cons of various combinations of switching sequences are compared and analyzed in [25]. The results show that the symmetrical switching sequence usually has a lower voltage distortion and less current ripple. Therefore, the symmetric switching mode is chosen in this paper. Moreover, in order to reduce the switching losses, it should be ensured that there is only one action at each switching state changing. Earlier in the article,

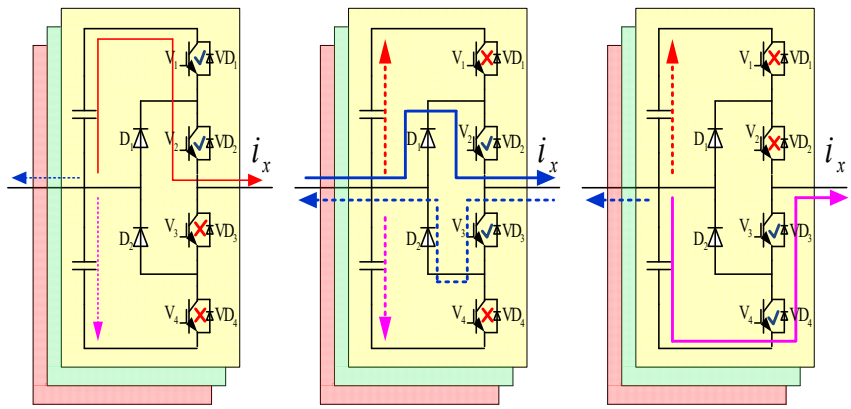

Fig. 6. Simplified model of the dc-link: (a) switching state "P"; (b) switching state "O"; (c) switching state "N".

the switch state [S_a, S_b, S_c] of the datum point vector V_A was obtained by an inverse coordinate transform. Therefore, the switch states of V_B, V_C, V_D can be obtained by a similar method. However, the matrix multiplication is complex and consumes a lot of system resources. Actually, in the case where the switching state of V_A is known, the other three switch states of V_B, V_C, V_D can be derived by judging the positional relationship of adjacent vertices. The rules are as follows:

a) If the two adjacent vertices locate on the planes of L=y (y=0, ±1, ±2), the switch states of the two corresponding basic vectors produce a state change in phase A along with the variation direction of the zero-sequence component. Taking points A and B in Fig. 4(h) as an example, adding one state to the switching state of V_A(ONN) in phase A obtain the switching state of V_B as PNN.

b) If the two adjacent vertices locate on the planes of K=y (y=0, ±1, ±2), the switch states of the two corresponding basic vectors produce a state change in phase B along with the variation direction of the zero-sequence component. Taking the two points B and C in Fig. 4(h) as an example, adding one to the state switching state of V_B(PNN) in phase B obtains the switching state of V_C as PON.

c) If the two adjacent vertices locate on the planes of K-L=y (y=0, ±1, ±2), the switch states of the two corresponding basic vectors produce a state change in phase C along with the variation direction of the zero-sequence component. In Fig. 4 (h), the switching state of V_C is PON, and the switching state of V_D is POO. On the other hand, there is only one switching action in each moment of the basic vector changing, when the switch sequence is in the order V_A, V_B, V_C and V_D.

D. Control on Neutral-Point Potential

The imbalance of the dc-link NP potential is a problem that must be considered and solved in three-level three-leg center-split capacitor inverters, otherwise it affects the waveform quality of the output voltage and threatens the safe operation of the power system. The influences of the switching state and the phase current on the NP potential [8] are illustrated in Fig. 6.

If i_x>0(x=a, b, c) and the switching state is "P", the upper capacitor discharges. However, the working state (discharge or charge) of the lower capacitor is a lot more complicated because it depends on the switching state of the other two phase legs and the zero sequence current of the system. When the switching state is "N" the lower capacitor charges and the working state of the upper capacitor becomes difficult to judge. However, since the switching state is "O" the current has no impact on the neutral-point potential. However, the upper and lower capacitors may charge or discharge, which is decided by the switching state and other two phase currents. On the other hand, if i_x<0, the result is opposite. Despite the fact that changes of NP potential are influenced by many factors, the current i_x has a decisive influences on the NP potential. Therefore, it is possible to implement the control on the NP potential by changing the switching states appropriately based on the phase current variation. In one basic unit the vectors V_A and V_D have the same K-axis and L-axis components. Thus, the reallocation of the duration time between them has a minimal influence on the constituted reference vectors [8].

For example, when the reference vector locates in the basic unit shown in Fig. 3(h) and u_{c1}> u_{c2} is satisfied, if i_a>0 and i_b+i_c<0, it only needs to increase the duration time of the switching state "POO" while reducing the duration time of the switching state "ONN". If i_a>0 and i_b+i_c>0, increasing the duration time of the switching states "ONN" and "POO" makes the neutral-point potential balanced. It does not need to be processed in this situation. If i_a<0 and i_b+i_c>0, reducing the duration time of the switching state "POO" and increasing the duration time of the switching state "ONN" makes the NP potential tend to be balance. However if i_a<0 and i_b+i_c<0, any change in the duration time between the switching states "POO" and "ONN" further exacerbates the imbalance. Although this condition rarely occurs in actual system operation, further study of the control method is still needed. By comparing the absolute values of i_a and i_b+i_c, the switching state corresponding to the bigger one is chosen and its duration

TABLE IV
SIMULATION PARAMETERS

Parameter	Value
Dc-link Voltage	600V
Dc-link Capacitor	2200uF
Switching Frequency	5kHz
Resistive–Inductive Load	R=8Ω, L=4mH
Modulation index	0.1<M<1
Unbalance degree	$0<\varepsilon_0<1$
Phase of zero-sequence component	$-\pi<\varphi_0<\pi$

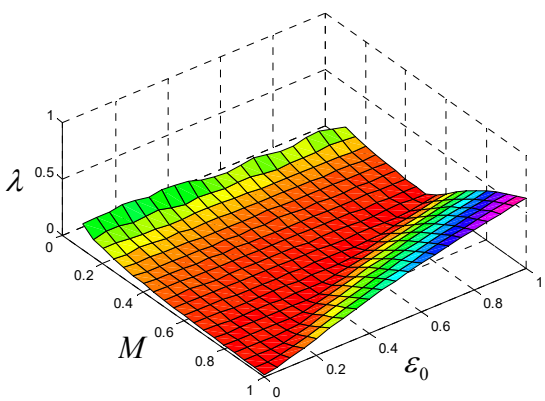

Fig. 7. Changing trend of the restoration degree λ with varied values of M and ε_0, when $\varphi_0 = 0$.

time should be increased to suppress further expansion of the neutral-point imbalance within the present switching period. In order to facilitate the adjustment of the duration time of V_A and V_D when the NP potential is unbalanced, a NP potential balance factor $f \in [0,1]$ is introduced in this paper. The adjusted duration time is expressed as equations (8) and (9).

If the duration time of V_A needs to be increased and that of V_D needs to be decreased, equation (8) is used to adjust the duration time. If not, equation (9) is used. Obviously the control of the NP potential unbalance is more effective with a smaller f. However, there is a greater zero sequence error in the output voltage at the same time. Therefore, appropriate values of the balance factor f are decided based on the specific situation of the unbalance of the NP potential.

$$\begin{cases} t_0^* = t_0 * f \\ t_4^* = t_4 + t_0 * (1-f) \end{cases} \tag{8}$$

$$\begin{cases} t_0^* = t_0 + t_4 * (1-f) \\ t_4^* = t_4 * f \end{cases} \tag{9}$$

IV. SIMULATION AND EXPERIMENT

A. Simulation Results

In three-phase four-wired multi-level converters, the output capability of the reference voltage is usually affected by the modulation index (M), the unbalance degree (ε_0) and the phase angle the of zero-sequence component (φ_0), where the

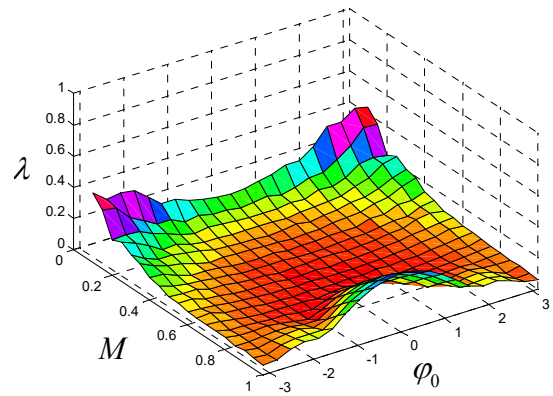

Fig. 8. Changing trend of the restoration degree λ with varied values of M and φ_0, when $\varepsilon_0 = 0.5$.

unbalance degree (ε_0) is defined as the ratio between the amplitude of the fundamental positive sequence component contained in the reference voltage and the amplitude of the zero-sequence component contained in the reference voltage. The phase (φ_0) is the initial phase of the zero-sequence component of the reference voltage.

Simulations have been carried out for the output performance of the reference voltage with the proposed non-orthogonal 3D-SVM under different values of M, ε_0 and φ_0 in the MATLAB\SIMULINK environment considering the parameters in Table IV.

To evaluate the output capability of the non-orthogonal 3D-SVM for the reference voltage in different cases, the restoration degree of the reference voltage λ is defined in equation (10).

$$\lambda = 1 - \frac{U_1}{U_{ref}} + \sqrt{\sum_{n=2}^{50} \frac{U_n^2}{U_1^2}} \tag{10}$$

Where, U_{ref} is the reference voltage amplitude, U_1 indicates the output fundamental voltage amplitude of the inverter, U_n is each of the harmonic amplitudes of the inverter output voltage, and $\sqrt{\sum_{n=2}^{50} \frac{U_n^2}{U_1^2}}$ represents the total harmonic voltage distortion within 50 orders. From equation (10), the inverter obtains the stronger output capability of the reference voltage when λ has a smaller value.

Fig. 7 shows the changing trend of the restoration degree λ varying with M and ε_0, when $\varphi_0 = 0$. When the unbalance degree is small (ε_0<0.3), the output capability of the reference voltage decreases with a reduction of M, and λ is primarily affected by harmonic distortion. With an increase of the unbalance degree, the output ability of the reference voltage is dramatically reduced in the high-modulation area (M>0.7).

However, the output ability of the reference voltage increases in low-modulation area (M<0.3).

Fig. 8 shows the changing trend of the restoration degree λ varying with M and φ_0, when $\varepsilon_0 = 0$. When the reference voltage in the moderate-modulation area (0.3<M<0.7), changes of φ_0 have little impact on the output capability and it is kept

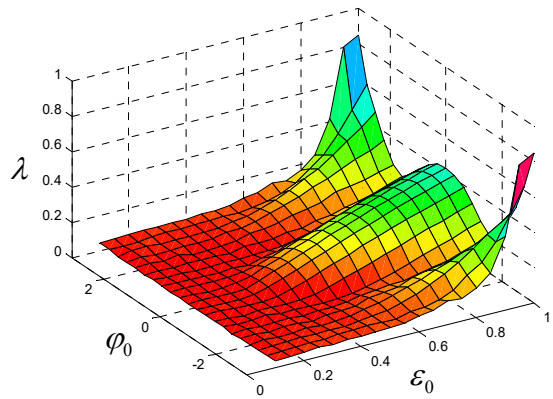

Fig. 9. Changing trend of the restoration degree λ with varied values of φ_0 and ε_0, when M= *0.8*.

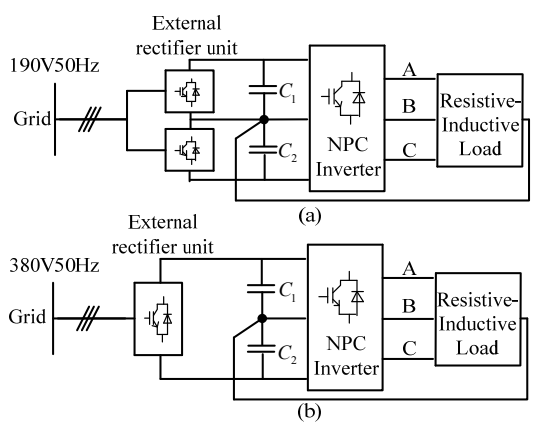

Fig. 10. Experimental prototype.

high. When the reference voltage is in the high-modulation area (M>0.7), the output capability of the reference voltage strengthens with an increase of φ_0. When the reference voltage is in the low-modulation area, the variation of output capability is opposite.

Fig. 9 shows the changing trend of the restoration degree λ varying with ε_0 and φ_0, when M = 0.8. When the unbalance degree is small (ε_0<30%), the changes of φ_0 have little impact on the reference voltage waveform and the restoration degree is high. If the unbalance degree exceeds 50%, the output capability of the reference voltage decreases from the phase angle ±π/2 in both directions.

B. Experimental Validation

To further verify the effectiveness of the proposed non-orthogonal 3D-SVM, an experimental platform was built as depicted in Fig. 10.

Experimental results obtained from the former prototype are utilized to evaluate the output ability of the reference voltage of the non-orthogonal 3D-SVM under different conditions. The latter prototype is developed to verify the strategy of the NP potential balance control. All of the experimental parameters are same as those of the simulation and shown in Table IV. An Agilent DSO-X3014A oscilloscope is applied to observe the system variables during the experiment and experimental data

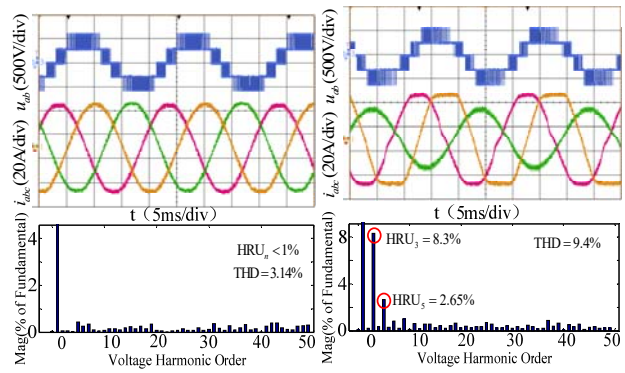

(a) ε_0 =0. (b) ε_0 =40%.

Fig. 11. Experimental waveform when M=1.

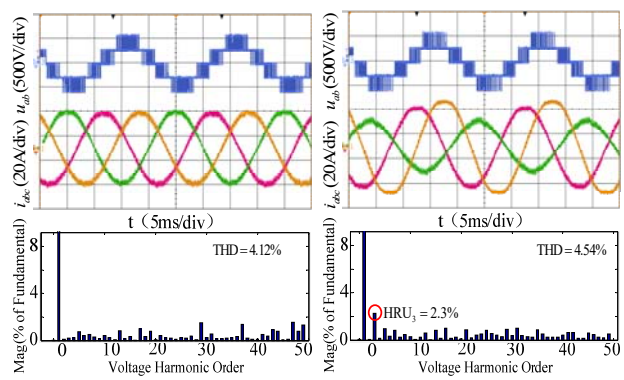

(a) ε_0 =0. (b) ε_0 =40%.

Fig. 12. Experimental waveform when M=0.8.

sampled by the oscilloscope at 100 kHz are imported into MATLAB for spectrum analysis.

Experimental results obtained from the former prototype are shown in Fig. 11, 12 and 13. Fig. 13 shows the line-to-line voltage of the inverter AC terminal u_{ab}, the three-phase load current i_{abc} and the spectrum of u_{ab} when M=1. In Fig. 12.(a), since the inverter works in the inversion state with balanced loads and reference voltage, the three-phase load current is balanced. The line-to-line voltage has five levels and the voltage total distortion rate (THD, considering only within fifty orders) is 3.14%. In Fig. 11(b), a zero-sequence component with ε_0=40% and φ_0=35° is added to the reference voltage. It can be seen that the load currents have obvious distortion. From the spectrum of u_{ab}, it is found that the line-to-line voltage contains a large number of 3rd and 5th harmonic components in this case and the THD=9.4%. When M=1, the zero-sequence component of the converter has a weak output performance. As a result, a reference voltage with a large unbalance degree does not realize the linear output.

Fig.12 shows the results of u_{ab}, i_{abc} and the spectrum of u_{ab} when M=0.8. As can be seen from Fig.13, the unbalanced instruction voltage enters linear modulation area with a decrease of the modulation index, and the load current has no obvious distortion under an unbalanced reference voltage. From the spectrum of u_{ab}, it is found that the 3rd and 5th

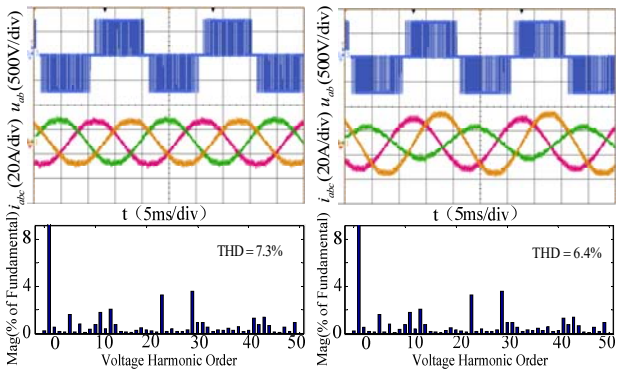

(a) ε_0 =0. (b) ε_0 =40%.

Fig. 13. Experimental waveform when M=0.5.

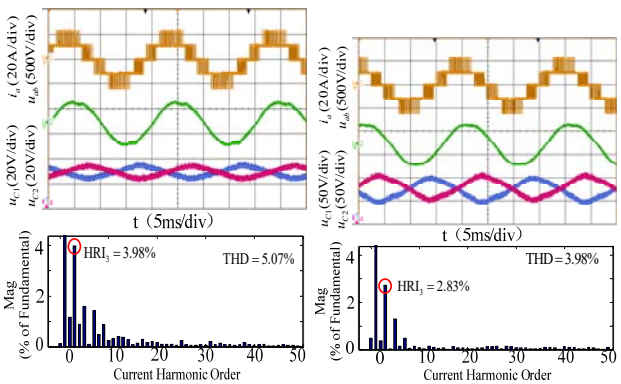

(a) f =0.5. (b) f =0.9.

Fig. 14. Experimental waveform when M=0.8.

harmonic components of u_{ab} decrease significantly when compared with the line-to-line voltage, when M=1 under an unbalanced instruction voltage. As shown in Fig. 13, when the modulation index is less than 0.5, the number of u_{ab} levels is reduced to three and there is a sharp increase in the total distortion of the output line-to-line voltage. However, with a decrease of the modulation index, the output performance of the zero-sequence voltage component is further improved.

Fig. 14 shows experimental waveforms with different NP balance factors for the unbalanced reference instruction voltage which is M=0.8 and ε_0=40%. When the reference instruction voltage is unbalanced, it produces a low-frequency pulsation in the NP potential of the inverter. Fig. 14(a) shows the upper and lower DC link voltages (u_{c1} and u_{c2}), the phase A current (i_a) and its spectrum when the balance factor is f=0.5. The maximum voltage difference between the upper and lower capacitors is 20V when f=0.5. In addition, an obvious distortion appears in the load current. The THD of i_a is 5.07%, and the proportion of the third harmonic in the fundamental frequency current is 3.98%. In Fig. 14(b), the maximum voltage difference between the upper and lower capacitors is 50V. The regulation on the duration time of V_A and V_D is relative weakening when f=0.9. However, the THD of i_a is 3.98%, and the proportion of the third harmonic is 2.83%. The smaller the balance factor of the NP potential is, the better its suppression

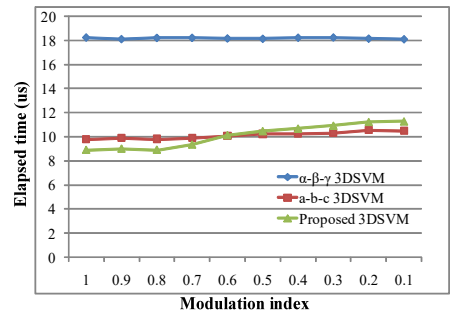

Fig. 15. Comparison of consumed time under different 3D-SVM strategies.

performance for the neutral-point potential fluctuation becomes, while the load current distortion increases. Therefore, an appropriate NP potential balance factor should be selected according to the actual situation.

Fig. 15 shows a comparison of the consumed time under different 3D-SVM strategies with the same Micro controller. The curves show that the time consumed by the conventional two 3D-SVM strategies are essentially unchanged throughout the entire modulation index. However, the time consumption of the proposed non-orthogonal 3D-SVM is increased with the decrease of the modulation index. This is due to the fact that the proposed 3DSVM strategy repeatedly corrects the basic unit with a decrease of modulation index. The time consumption of the proposed non-orthogonal 3D-SVM is shorter than that of the α-β-γ 3D-SVM and it is close to that of the a-b-c 3D-SVM. However, the proposed 3D-SVM strategy is better than the 3D-SVM based on the a-b-c coordinate system in the control of zero-sequence component.

V. CONCLUSIONS

A non-orthogonal 3D-SVM strategy that is suitable for multi-level TLSC inverters is proposed in this paper. The novel 3D-SVM works in a new non-orthogonal 3D coordinate system which integrates the advantages of two types of traditional three-dimensional coordinate systems. The equivalence between the proposed non-orthogonal 3D coordinate system and the traditional 3D orthogonal coordinate systems has been derived and verified by an affine transform. The proposed non-orthogonal 3D-SVM converts the trigonometric functions in the α-β-γ 3D-SVM into simple algebraic operations, which greatly reduces the algorithm complexity of the 3D-SVM. On the other hand, the non-orthogonal 3D-SVM has the decoupling expression of the symmetrical and asymmetrical components of the reference voltage. Therefore, it has better capability of zero sequence independent and NP balanced control than the a-b-c 3D-SVM. In addition, considering the inherent NP potential unbalance issue of three-level TLSC inverters, a simple control strategy was added to the non-orthogonal 3D-SVM. Finally, numerous experiments have verified the correctness and effectiveness of the proposed 3D-SVM.

ACKNOWLEDGMENT

This work has been supported by the National Natural Science Foundation of China under Award 51407183.

REFERENCES

[1] N. Y. Dai, M. C. Wong, and Y. D. Han, "Three-dimensional space vector modulation with DC voltage variation control in a three-leg center-split power quality compensator," *IEE Proceedings – Electric Power Applications*, Vol. 151, No. 2, pp. 198–204, Mar. 2004.

[2] N. Y. Dai, M. C. Wong, and Y. D. Han, "Application of a three-level NPC inverter as a three-phase four-wire power quality compensator by generalized 3DSVM," *IEEE Trans. Power Electron.*, Vol. 21, No. 2, pp. 440–449, Mar. 2006.

[3] X. P. Yang, Y. X. Zhang, and Y. R. Zhong, "Three-phase four-wire DSTATCOM based on a three-dimensional PWM algorithm," in *Third International Conference on Electric Utility Deregulation and Restructuring and Power Technologies (DRPT)*, pp. 2061-2066, Apr. 2008.

[4] L. H. Zhu, Y. Zou, X. Zou, S. Chao, J. Tang, X. She, and Z. Zhang, "A novel 3-d space vector modulation scheme for three-level three-leg NPC converter in three-phase four-wire APF system," in *Energy Conversion Congress and Exposition (ECCE)*, pp. 1527–1532, Sep. 2012.

[5] J. Tang, X. D. Zou, X, She, and Y. P. Zou, "A research on neutral-point potential balancing control strategy for three-phase four-wire tri-level three-leg APFs," *Proceedings of the CSEE*, Vol. 29, No. 24, pp. 40–48, Aug. 2009.

[6] M. M. Prats, L. G. Franquelo, J. I. Leon, R. Portillo, E. Galvan, and J. M. Carrasco, "A SVM-3D generalized algorithm for multilevel converters," in *The 29th Annual Conference of the IEEE Industrial Electronics Society (IECON)*, pp. 24–29, Nov. 2003.

[7] J. Tang, X., Zou, Y. Xu, X. She, Z. Bo, and Y. Zou, "Novel 3-DSVM scheme for three-phase four-wire tri-level APFs," in *IEEE 6th International Power Electronics and Motion Control Conference (IPEMC),* pp. 882-886, May 2009.

[8] N. Y. Dai, M. C. Wong, Y. D. Han, and C. S. Lam, "A 3-D generalized direct PWM for 3-phase 4-wire APFs," in *Fourtieth IAS Annual Meeting. Conference Record of the 2005 Industry Applications Conference,* pp. 1261-1266, Oct. 2005.

[9] X. S. Li, Z. Deng, Z. Chen, and Q. Fei, "Analysis and simplification of three-dimensional space vector PWM for three-phase four-leg inverters," *IEEE Trans. Ind. Electron.*, Vol. 58, No. 2, pp. 450–464, Feb. 2011.

[10] B. Singh and S. Sharma, "Design and implementation of four-leg voltage source-converter-based VFC for autonomous wind energy conversion system," *IEEE Trans. Ind. Electron.*, Vol. 59, No. 12, pp. 4694–4703, Dec. 2012.

[11] S. Albatran, Y. Fu, A. Albanna, R. Schrader, and M. Mazzola, "Hybrid 2D-3D space vector modulation voltage control algorithm for three phase inverters," *IEEE Trans. Sustain. Energy*, Vol. 4, No. 3, pp. 734–744, Jul. 2013.

[12] M. Zhang, D. J. Atkinson, B. Ji, M. Armstrong, and M. Ma, "A near state three-dimensional space vector modulation for a three-phase four-leg voltage source inverter," *IEEE Trans. Power Electron.*, Vol. 29, No. 11, pp. 5715–5726, Nov. 2014.

[13] J. Chivite-Zabalza, P. Izurza-Moreno, D. Madariaga, G. Calvo, and M. A. Rodriguez, "Voltage balancing control in 3-level neutral-point clamped inverters using triangular carrier PWM modulation for FACTS applications," *IEEE Trans. Power Electron.*, Vol. 28, No. 10, pp. 4473–4484, Oct. 2013.

[14] L. M. Tolbert and T. G. Habetler, "Novel multilevel inverter carrier-based PWM method," in *Thirty-Third IAS Annual Meeting. Industry Applications Conference*, Oct. 1998.

[15] Y. Cho, T. LaBella, J. S. Lai, and M. K. Senesky, "A carrier-based neutral voltage modulation strategy for multilevel cascaded inverters under unbalanced DC Sources," *IEEE Trans. Ind. Electron.*, Vol. 61, No. 2, pp. 625–636, Feb. 2014.

[16] Y. Jiao, F. C. Lee, and S. Lu, "Space vector modulation for three-level NPC converter with neutral point voltage balance and switching loss reduction," *IEEE Trans. Power Electron.*, Vol. 29, No. 10, pp. 5579–5591, Oct. 2014.

[17] W. D. Jiang, S. W. Du, L. C. Chang, Y. Zhang, and Q. Zhao, "Hybrid PWM strategy of SVPWM and VSVPWM for NPC three-level voltage-source inverter," *IEEE Trans. Power Electron.*, Vol. 25, No. 10, pp. 2607–2619, Oct. 2010.

[18] J. H. Seo, C. H. Choi, and D. S. Hyun, "A new simplified space–vector PWM method for three-level inverters," *IEEE Trans. Power Electron.*, Vol. 16, No. 4, pp. 545–550, Jul. 2001.

[19] B. P. McGrath, D. G. Holmes, and T. Meynard, "Reduced PWM harmonic distortion for multilevel inverters operating over a wide modulation range," *IEEE Trans. Power Electron.*, Vol. 21, No. 4, pp. 941–949, Jul. 2006.

[20] J. N. Chiasson, L. M. Tolbert, K. J. McKenzie, and Z. Du, "A unified approach to solving the harmonic elimination equations in multilevel converters," *IEEE Trans. Power Electron.*, Vol. 19, No. 2, pp. 478–490, Mar. 2004.

[21] C.-C. Hou, C.-C. Shih, P.-T. Cheng, and A. M. Hava, "Common-mode voltage reduction pulse width modulation techniques for three-phase grid connected converters," *IEEE Trans. Power Electron.*, Vol. 28, No. 4, pp. 1971–1979, Apr. 2013.

[22] G. I. Orfanoudakis, M. A. Youratich, and S. M. Sharkh, "Hybrid modulation strategies for eliminating low-frequency neutral-point voltage oscillations in the neutral-point-clamped converter," *IEEE Trans. Power Electron.*, Vol. 28, No. 8, pp. 3653–3658, Aug. 2013.

[23] M. C. Wong, Z. Y. Zhao, Y. D. Han, and L. B. Zhao, "Three-dimensional pulse-width modulation technique in three-level power inverters for three-phase four-wired system," *IEEE Trans. Power Electron.*, Vol. 16, No. 3, pp. 418–427, May 2001.

[24] M.-C. Wong, J. Tang, and Y. D. Han, "Cylindrical coordinate control of three-dimensional PWM technique in three-phase four-wired tri-level inverter," *IEEE Trans. Power Electronics*, Vol. 18, No. 1, pp. 208–220, Jan. 2003.

[25] J. H. Kim and S. K. Sul, "A carrier-based PWM method for three phase four-leg voltage source converters," *IEEE Trans. Power Electron.*, Vol. 19, No. 1, pp. 66–75, Jan. 2004.

[26] A. Mohd, E. Ortjohann, N. Hamsic, W. Sinsukthavorn, M. Lingemann, A. Schmelter, and D. Morton, "Control strategy and space vector modulation for three-leg four-wire voltage source inverters under unbalanced load conditions," *IET Power Electronics*, Vol. 3, No. 3, pp. 323–333, May 2010.

[27] E. Ortjohann, A. Mohd, N. Hamsic, and M. Lingemann, "Design and experimental investigation of space vector modulation for three-leg four-wire voltage source inverters," in *13th European Conference on Power Electronics and Applications (EPE)*, pp. 1–6, Sep. 2009.

[28] T. H. Nguyen, P. K. W. Chan, Y. Shrivastava, and S. Y. R. Hui, "A three-dimensional space vector modulation scheme for three-level three-wired neutral point clamped converters," in *IEEE 36th Power Electronics Specialists Conference (PESC)*, pp. 2307–2314, Jun. 2005.

[29] M. M. Prats, J. M. Carrasco, and L. G. Franquelo, "Effective algorithm for multilevel converter with very low computational cost," *Electronics Letters,* Vol. 38, No. 22, pp. 1398–1400, Oct. 2002.

[30] M. M. Prats, L. G. Franquelo, R. Portillo, J. I. Leon, E. Galvan, and J. M. Carrasco, "A 3-D space vector modulation generalized algorithm for multi-level converters," *IEEE Power Electron. Lett.*, Vol. 1, No. 4, pp. 110–114, Dec. 2003.

[31] N. Y. Dai, M. C. Wong, Y. H. Chen, and Y. D. Han, "A 3-D generalized direct PWM algorithm for multilevel converters," *IEEE Power Electron. Lett.*, Vol. 3, No. 3, pp. 85–86, Sep. 2005.

[32] N. Y. Dai, M. C. Wong, F. Ng, and Y. D. Han, "A FPGA-based generalized pulse width modulator for three-leg center-split and four-leg voltage source inverters," *IEEE Trans. Power Electron.*, Vol. 23, No. 3, pp. 1472–1484, May 2008.

[33] X. Liu, Y. X. Xie, and Y. Wang, "A simplified 3D-SVPWM algorithm for three-phase four-wire shunt active power filter," in *17th International Conference on Electrical Machines and Systems (ICEMS)*, pp. 1457–1462, Oct. 2014.

[34] S. Albatran, Y. Fu, and A. Albanna, "Comprehensive mathematical description and harmonic analysis of hybrid 2D-3D space vector modulation," *IEEE Trans. Ind. Electron.*, Vol. 61, No. 7, pp. 3327–3336, Jul. 2014.

[35] R. Zhang, V. H. Prasad, D. Boroyevich, and F. C. Lee, "Three-dimensional space vector modulation for four-leg voltage-source converters," *IEEE Trans. Power Electron.*, Vol. 17, No. 3, pp. 314–326, May 2002.

Chuanjin Zhang was born in Xuzhou, China, in 1986. He received his B.S. degree from the School of Electrical Engineering, Northeast Dianli University, Jilin, China, in 2009; and his M.S. degree in Power Electronics and Drives from the China University of Mining and Technology, Xuzhou, China, in 2012, where he is presently working towards his Ph.D. degree in the School of Information and Electrical Engineering. His current research interests include power quality compensation systems, motor control and power electronics.

Rui-Peng Wei was born in Xingtai, China, in 1990. He received his B.S. degree in Electrical Engineering from the China University of Mining and Technology, Xuzhou, China, in 2015, where he is presently working towards his M.S. degree in Electrical Engineering. His current research interests include power quality and power system analysis.

Yi Tang was born in Zhangjiagang, China, in 1957. He received his Ph.D. degree from the School of Information and Electrical Engineering, China University of Mining and Technology, Xuzhou, China, in 1995. He is presently working as a Professor in the China University of Mining and Technology. His current research interests include power quality and power system analysis.

Ke Wang was born in Xuzhou, China, in 1985. He received his B.S. degree in Electrical Engineering and Automation and his M.S. degree in Power Electronics and Drives from the China University of Mining and Technology, Xuzhou, China, in 2005 and 2009, respectively; where he is presently working towards his Ph.D. degree in the School of Information and Electrical Engineering. His current research interests include power electronic converters, active power filters and fault diagnosis.